ORIGINAL RESEARCH ARTICLE

Process Optimization and Influencing Factors of Supersonic High-Energy Plasma Spraying of Al$_2$O$_3$-PF Composite Coatings on Polymer Matrix Composite Surface

Ming Liu[1] · Qi-qing Peng[2] · Yan-fei Huang[1] · Guo-zheng Ma[1] · Wei-ling Guo[1] ·
Hai-dou Wang[1,3] · Xuan-ping Luo[2] · Wei Lang[2]

Abstract A high-performance Al$_2$O$_3$-PF composite coating was prepared on the surface of polymer matrix composite materials using supersonic high-energy plasma spraying technology. The bonding strength between the composite coating and the matrix was used as the evaluation index. The spraying process parameters were optimized using orthogonal experimental design method. Subsequently, the optimal process was verified based on single-factor experimental method, further exploring the influence mechanism of Ar flow rate, spraying current, spraying voltage, and second powder feeding position on the composite coating. Analysis shows that spray voltage, Ar flow rate, and spray current have a significant impact on the experimental results and are the main influencing factors; the second powder feeding position has a relatively small impact on the experimental results and is a secondary influencing factor.

Keywords Al$_2$O$_3$-PF composite coating · bonding strength · orthogonal test · polymer matrix composite · resin matrix protective coating · supersonic plasma spraying

✉ Qi-qing Peng
1371090419@qq.com

1 National Key Laboratory for Remanufacturing, Army Academy of Armored Forces, Beijing 100072, China

2 PLA 77626 Force, Lasa, China

3 National Engineering Research Center for Remanufacturing, Army Academy of Armored Forces, Beijing 100072, China

Introduction

Polymer matrix composites are characterized by low density, high specific modulus and specific strength (Ref 1), good vibration damping performance (Ref 2, 3), and excellent designability (Ref 4-6) and dielectric properties (Ref 7) as compared to traditional structural materials such as metals. Therefore, polymer matrix composites have been widely used in high-end fields such as national defense and aerospace (Ref 8). It is worth noting that as polymer materials, polymer matrix composites have unsatisfactory high-temperature resistance, erosion resistance, electrical conductivity and wear resistance, which restricts their further application in industrial production, scientific research and other fields (Ref 9).

To solve the above problems, researchers in both China and abroad have carried out a lot of fruitful research on improving the surface properties of polymer matrix composites, especially by using additional functional coatings. For example, M.Ivosevic et al. (Ref 10-14) used the high-velocity oxygen fuel (HVOF) technique to spray polymer/cermet functional gradient coatings on the surfaces of polymer matrix composites to improve the solid particle erosion resistance of composites. Tian Haoliang et al. (Ref 15) deposited Y$_2$O$_3$ partially stabilized ZrO$_2$ (YSZ)-based thermal barrier coatings (TBCs) on the surfaces of polyimide matrix composites by explosive spraying, which effectively enhanced the heat resistance of composites. Aiguo Liu et al. (Ref 16-18) used steel strip-coated Ni-Cr-B-Si powder as the wire material of arc spraying and deposited a single-layer coating and a double-layer coating (using Zn as the bonding layer) on the surfaces of graphite fiber-reinforced polyimide composites. They found that both coatings could improve the high-temperature resistance and erosion resistance of composites, the bonding

strength of coatings reached 9.4 MPa and 9.3 MPa, respectively, and the thermal shock cycle was up to 45 and 49 times, respectively. Moreover, Kazuhisa Miyoshi et al. (Ref 19) deposited WC-Co coating on the metal bonding layer on the polymethyl methacrylate surface by plasma spraying, which enhanced the particle erosion resistance of the matrix by about 10 times and effectively prolonged the service life of the composites.

Our research group had explored the preparation of aluminum oxide-phenolic resin (Al_2O_3-PF) composite coating on the surface of polymer matrix composite by supersonic high-energy plasma spraying, and achieved remarkable results. The prepared Al_2O_3-PF composite coating not only possessed good bonding strength with the polymer matrix, but also provided excellent ablation resistance for the matrix. Meanwhile, the co-deposition mechanism of high-melting-point ceramic particles and low-thermal-decomposition-temperature resin particles was analyzed to reveal the construction mechanism of Al_2O_3-PF composite coatings (Ref 20, 21).

Based on the preliminary work of our research group, the mechanism of spraying factors on the construction and properties of Al_2O_3-PF composite coatings during supersonic high-energy plasma spraying was further explored using the orthogonal test and single-factor test in this paper.

Overview of Orthogonal Test Design and Data Analysis

Orthogonal test design is an efficient, economical and fast test design method for studying multi-factors and multi-levels. According to orthogonality, some representative tests are selected from the all-factor test mix and combined into a test scheme, which can effectively reduce the test workload and comprehensively reflect the influence degree of each test factor on the assessment indicators (Ref 22).

The orthogonal array is expressed as L_n (a^b). For example, four-factor and three-level L_9 (3^4) is an orthogonal array (L) with 9 rows (i.e., the runs of orthogonal tests), 3 levels of each factor in the array and 4 columns (i.e., the number of test factors that can be designed at most in the array), as shown in Tables 1 and 2.

After the orthogonal test design is completed, all tests should be completed in strict accordance with the corresponding test scheme, during which the test order can be changed to eliminate the influences of some uncertainties on the test results. After all tests are completed, the test data are analyzed usually by intuitive analysis and range analysis (Ref 23).

To facilitate the calculation and analysis of orthogonal test data, the following symbols are introduced:

K_{ij}- the sum of all test results at level i in the j-th column;

$\overline{K_{ij}}$- the mean of all test results at level i in the j-th column;

R_j- the range of the j-th column (i.e., the maximum of $\overline{K_{ij}}$ minus the minimum of $\overline{K_{ij}}$ in the j-th column).

R_j can indicate the importance of the influences of the test factor on the test results, that is, the higher the value of R_j, the more significant the influences of the factor on the test results, which is the primary factor. In contrast, the lower the value of R_j, the less the influences of the factor on the test results, which is the secondary factor.

Process Optimization with Bonding Strength as an Assessment Indicator

There is an interface bonding of heterogeneous materials between the Al_2O_3-PF composite coating and the polymer matrix, dominated by mechanical meshing, and the reliable coating-matrix bonding is also the basis and premise of the

Table 1 Factors and horizontal design of L_9 (3^4) orthogonal experiment

Levels	Factors			
	A	B	C	D
1	A_1	B_1	C_1	D_1
2	A_2	B_2	C_2	D_2
3	A_3	B_3	C_3	D_3

Table 2 L_9 (3^4) orthogonal experiment table and data analysis

Levels	Factors				Evaluating indicator
	A	B	C	D	
1	A_1	B_1	C_1	D_1	
2	A_1	B_2	C_2	D_2	
3	A_1	B_3	C_3	D_3	
4	A_2	B_1	C_2	D_3	
5	A_2	B_2	C_3	D_1	
6	A_2	B_3	C_1	D_2	
7	A_3	B_1	C_3	D_2	
8	A_3	B_2	C_1	D_3	
9	A_3	B_3	C_2	D_1	
K_{1j}					
K_{2j}					
K_{3j}					
$\overline{K_{1j}}$					
$\overline{K_{2j}}$					
$\overline{K_{3j}}$					
R_j					

protective effect of coatings, so the bonding strength was taken as a preliminary basic assessment indicator in the orthogonal test design.

It should be noted that the microstructure of the pure Al_2O_3 and Al_2O_3/PF composite powder used in the experiment is shown in Fig. 1. From Fig. 1, it can be observed that pure Al_2O_3 powder has very good sphericity, with a powder particle size of 15-50 μm. Suitable for plasma spraying; Compared to others, Al_2O_3/PF composite powders are mainly irregularly shaped and have a wide particle size distribution (approximately 0.2-100 μm) Among them, small particles (particle size ranging from 0.2 to 10 μm) The main reason for the formation of Al_2O_3/ PF composite powder is that it is a coated powder obtained by agglomeration of Al_2O_3 and PF resin, resulting in the detachment of some small particles adsorbed on the surface of large particles during storage, transportation, and other processes.

As found in a large number of preliminary investigations, the Al_2O_3-PF composite coating prepared using the process parameters shown in Table 3 (Ref 20) possessed excellent mechanical properties (with a maximum bonding strength of 28.1 MPa). In addition, four influencing factors for process parameters of Al_2O_3-PF composite coating

deposition were found: the second powder feeding position (mm), Ar flow rate (L min^{-1}), spraying voltage (V) and spraying current (A). Therefore, the tests in this paper were carried out based on the preliminary investigations, and the L_9 (3^4) orthogonal array was further designed. The test parameters are shown in Table 4.

According to the above-mentioned orthogonal test design, a four-factor and three-level orthogonal array of supersonic high-energy plasma spraying of Al_2O_3-PF composite coatings was designed, and the test data were analyzed, as shown in Table 5.

The following preliminary conclusions could be drawn from the data analysis of Table 5:

1. Data analysis of bonding strength
   The bonding strength ranged from 14.2 to 23.8 MPa among the 9 groups of tests, which was slightly lower than that in the preliminary investigation but still reached above 20 MPa.
2. Data analysis of factor range
   R_j of the second powder feeding position, Ar flow rate, spraying voltage and spraying current was 0.83, 4.73, 5.57 and 2.87, respectively, in the tests. It can be seen that spraying voltage, Ar flow rate and spraying current had great influences on the test results, which were the
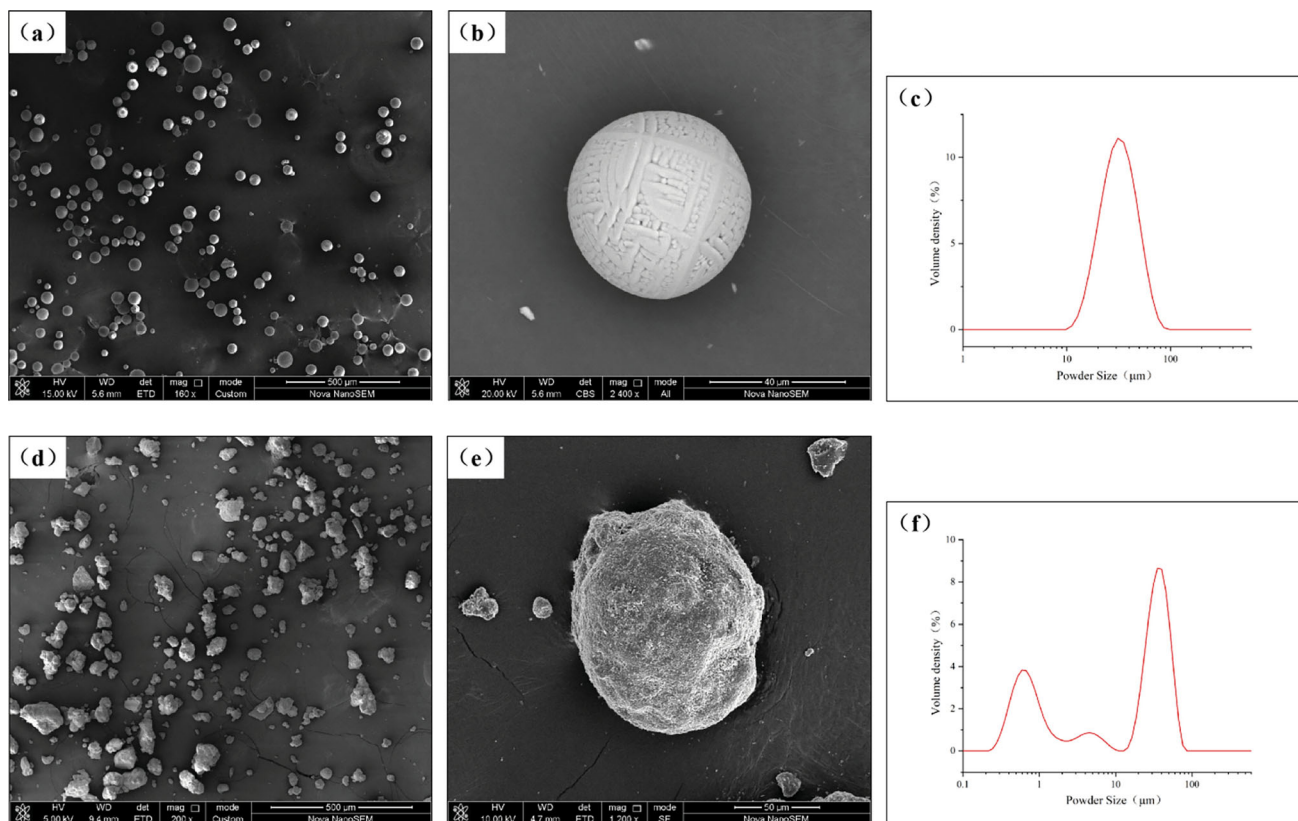
Fig. 1 SEM morphology and particle size distribution of two types of spray powders: (a-c) pure Al_2O_3 powder; (d-f) Al_2O_3/PF composite powder

Table 3 Supersonic plasma spray process parameters (Ref 20)

Spray parameters Powder delivery method	Spraying materials	
	Spherical pure Al$_2$O$_3$ powder Internal powder delivery	Al$_2$O$_3$/PF composite powder External powder delivery
Spray current, A	420	420
Spray voltage, V	110	110
Argon gas flow rate, L/min	60	60
Hydrogen flow rate, L/min	22	22
Spraying distance, mm	150	50
Powder feed rate, g/min	7	7.5
Pressure of powder delivery gas, MPa	0.4	0.45
Gas flow rate for conveying powder, L/min	15	15
Injection angle θ, °	…	90
Axial distance a, mm	…	100
Radial distance r, mm	…	2.5
Substrate temperature, °C	130 ± 10	

Table 4 Selection of process parameters for four-factor three-level orthogonal experiments

Levels	Factors			
	A Second powder feeding position, mm	B Argon gas flow rate, L min^{-1})	C Spray voltage, V	D Spray current, A
1	40	50	100	410
2	50	60	110	420
3	60	70	120	430

primary influencing factors, while the second powder feeding position had little influence on the test results, which was the secondary influencing factor. Therefore, the influences of spraying voltage, Ar flow rate and spraying current on the coating deposition and properties were the focuses in the subsequent tests, and the second powder feeding position was set at 60 mm and its influences on the test results were ignored.

3. Two groups of optimal parameter combinations with bonding strength as an assessment indicator
First, the tested optimal combination was C$_2$B$_2$D$_2$ (the second group of test): spraying voltage of 110 V, Ar flow rate of 60 L min^{-1} and spraying current of 420 A, achieving a bonding strength of 23.8 MPa. It was found that without regard to the second powder feeding position, the process parameters in this combination were the same as those in the preliminary test, which can be considered as validation of the preliminary test. Second, the theoretical optimal combination was C$_2$B$_2$D$_1$: spraying voltage of 110 V, Ar flow rate of 60 L min^{-1} and spraying current of 410 A.

Therefore, C$_2$B$_2$D$_1$ was used as the optimal process for preparation of composite coatings in the subsequent tests, as shown in Table 6.

The influences of test factors on the bonding strength of Al$_2$O$_3$-PF composite coating is intuitively displayed in the intuitive analysis chart in Fig. 2 drawn based on the test data in Table 5. It was found that the coating bonding strength rose with the increase in the distance of the second powder feeding position (i.e., the powder feeding position was closer to the nozzle). However, the preliminary test showed that when the Al$_2$O$_3$-PF composite powder was too close to the nozzle, massive ablation of PF would occur due to the high jet temperature, and the second powder feeding position had little influence on the bonding strength. Therefore, it was reasonable to set the second powder feeding position at 60 mm.

Validation of Optimal Process and Analysis on Influence Mechanism on Coating Deposition by Single-Factor Test

To further validate the reliability of the theoretical optimal process and explore the influence mechanism of each factor on the deposition process of Al$_2$O$_3$-PF composite coating, a single-factor test based on the theoretical optimal combination was designed while ensuring test safety.

Table 5 Four-factor three-level orthogonal experimental design and result analysis of Al_2O_3-PF composite coating

Test number and other projects	A Second powder feeding position, mm	B Argon gas flow rate, L min^{-1}	C Spray voltage, V	D Spray current, A	Average bonding strength, MPa	Measurement standard deviation, MPa
1	40	50	100	410	14.2	2.55
2	40	60	110	420	23.8	1.83
3	40	70	120	430	16.2	2.19
4	50	50	110	430	17.0	2.12
5	50	60	120	410	23.2	1.77
6	50	70	100	420	14.3	2.48
7	60	50	120	420	18.5	1.73
8	60	60	100	430	16.9	1.51
9	60	70	110	410	21.3	2.03
K_{1j}	54.20	49.70	45.40	58.70		
K_{2j}	54.50	63.90	62.10	56.60		
K_{3j}	56.70	51.80	57.90	50.10		
$\overline{K_{1j}}$	18.07	16.57	15.13	19.57		
$\overline{K_{2j}}$	18.17	21.30	20.70	18.87		
$\overline{K_{3j}}$	18.90	17.27	19.3	16.70		
Range R_j	0.83	4.73	5.57	2.87		
Factor priority	C > B > D > A					
Superior level	60	60	110	410		

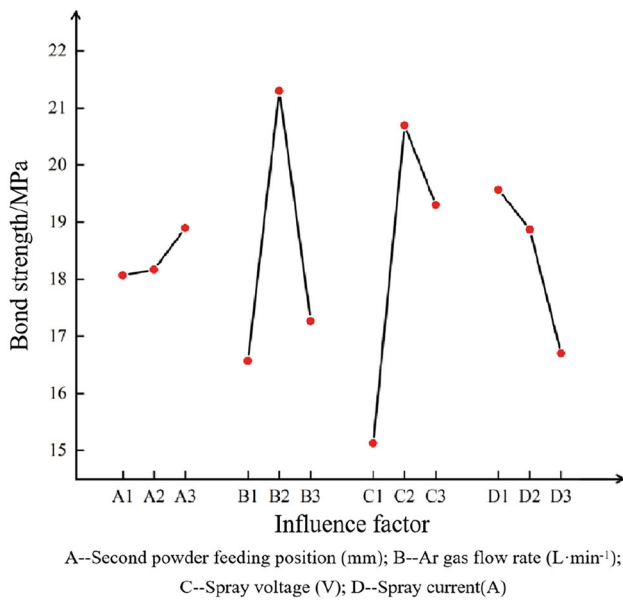**Table 6** Optimal process for supersonic high-energy plasma spraying of Al_2O_3-PF composite coatings

Spray parameters	Spraying materials	
Powder delivery method	Spherical pure Al_2O_3 powder Internal powder delivery	Al_2O_3/PF composite powder External powder delivery
Spray current, A	410	410
Spray voltage, V	110	110
Argon gas flow rate, L/min	60	60
Hydrogen flow rate, L/min	22	22
Spraying distance, mm	150	60
Powder feed rate, g/min	7	7.5
Pressure of powder delivery gas, MPa	0.4	0.45
Gas flow rate for conveying powder, L/min	15	15
Injection angle θ (°)	…	90
Axial distance a, mm	…	100
Radial distance r, mm	…	2.5
Substrate temperature, °C	130 ± 10	

Test Design and Result Analysis

Based on the analysis of the test data in "Process optimization with bonding strength as an assessment indicator" section, a theoretical optimal combination-based single-factor spraying scheme was designed for spraying voltage, Ar flow rate and spraying current. The process parameters and schemes in Table 7 were explored and validated, among which Scheme 2 was the theoretical optimal combination. Moreover, the bonding strength of the prepared composite coating was tested, and the results are shown in Table 8.

According to the analysis of test results, the following aspects warrant attention:

A--Second powder feeding position (mm); B--Ar gas flow rate (L·min⁻¹);
C--Spray voltage (V); D--Spray current(A)

Fig. 2 Visual analysis of four-factor three-level orthogonal experiment for Al_2O_3-PF composite coating

1. The bonding strength of composite coatings was significantly improved

   The mean bonding strength reached 20 MPa only in 3 out of the 9 groups of tests in Table 5. After optimization, the mean bonding strength was stable above 20 MPa in 7 groups of tests in Table 8, near 30 MPa at most. It suggests that the process of supersonic plasma spraying of Al_2O_3-PF composite protective coating on the surfaces of polymer matrix composites (epoxy resin matrix was used in this paper) was established and the ranges of parameters were reasonable and correct.

2. The quality of composite coatings greatly fluctuated

   Generally, the same group of coating samples should have the same structure and properties. However, it was found from the test results in Table 8 that the bonding strength had a great difference even in the same group of coating samples due to the particularity of the resin material, such as Scheme 1 and Scheme 6 in Fig. 3.

3. (3) The properties of epoxy resin matrix had obvious influence

   The molecular chain linking of polymers mainly depends on van der Waals force, which is sensitive to temperature. In a high-temperature environment, the structure and properties of polymer matrix composites will change quickly and significantly. Specifically, the mean temperature of particle jet measured during supersonic high-energy plasma spraying of spherical pure Al_2O_3 powder could reach 2900 °C, far higher than the tolerable temperature of resin materials.

Therefore, although the cooling device and process had been perfected, differences inevitably existed in the heating status of samples in the spraying process, leading to differences in the properties among coating and matrix samples. In addition, artificial differences in the blasting pretreatment of the matrix prior to spraying would also cause different changes in the structure of the matrix surface, as shown in Fig. 4.

As can be seen from Fig. 4, although the five coating samples prepared in Scheme 1 belonged to the same group, obvious differences were found in the macroscopic morphology and structure of the matrix and the coating. As shown in Fig. 1-1(a) and 1-2(a), the ablated areas (blackened areas) resulting from continuous heat accumulation during spraying were clearly larger and darker than those in Fig. 1-3(a), 1-4(a) and 1-5(a), indicating more severe ablation.

It should be pointed out that such ablation was not limited to the surface layer of the resin matrix, but also included PF in the deposited coating. Besides, the morphology of the five samples (Fig. 1-1(b) ∼ 1-5(b)) on the coating side was observed, and a surface resin with the resin matrix was found at the edge of each sample, suggesting the close bonding between the coating and the matrix surface. The residual resin surface areas of Fig. 1-1(b) and 1-2(b) were significantly smaller than those of Fig. 1-3(b), 1-4(b) and 1-5(b), indicating that the coating-matrix bonding of the former two was weaker than that of the latter three, consistent with the results in Table 8.

Influences of Ar Flow Rate (L min⁻¹)

Generally, as the major gas of plasma spraying, Ar plays two roles: First, it provides protection for the plasma spraying gun, so there is a minimum safe value for the Ar flow rate. In this paper, the Ar flow rate was at least 50 L/min to ensure the safety of the spraying process; second, the Ar flow rate can be adjusted to regulate the particle flight velocity, so that molten drops have enough kinetic energy to impinge the matrix to form flakes. Therefore, changes in particle velocity are more responsive to changes in the Ar flow rate, as shown in Fig. 5.

The influence rule of Ar flow rate on spraying of spherical pure Al_2O_3 powder is shown in Fig. 5 (Notes: due to an external feeding mode of Al_2O_3-PF composite powder, and large differences in powder shape and particle size, regular particle jet cannot form, and the particle flight information cannot be obtained using particle online monitoring system. Therefore, all data on particle flight state in this paper belonged to the jet from spherical pure

Table 7 Experimental scheme for verifying the optimal process of preparing Al_2O_3-PF composite coatings based on single-factor experiments

Experimental factors		A Argon gas flow rate, L min^{-1}	B Spray voltage, V	C Spray current, A	D Second powder feeding position, mm
Experimental parameters	I	50	105	400	60
	II	60	110	410	
	III	70	115	420	
Experimental plan	1	50	110	410	60
	2	60	110	410	
	3	70	110	410	
	4	60	105	410	
	5	60	115	410	
	6	60	110	400	
	7	60	110	420	

Table 8 Bond strength test results of Al_2O_3-PF composite coatings deposited under different spraying schemes

Spray coating scheme	Bond strength, MPa						Measurement standard deviation, MPa
	1	2	3	4	5	Average value	
1	19.8	18.1	25.8	24.5	24.3	22.50	2.99
2	27.6	31.2	27.0	32.2	30.0	29.60	2.01
3	26.3	27.3	23.5	25.2	24.1	25.28	1.39
4	26.3	27.7	26.6	29.9	25.7	27.24	1.48
5	25.2	25.1	27.0	28.4	29.6	27.06	1.76
6	23.1	27.0	30.7	22.1	29.1	26.40	3.33
7	20.8	24.8	22.6	25.2	27.0	24.08	2.16
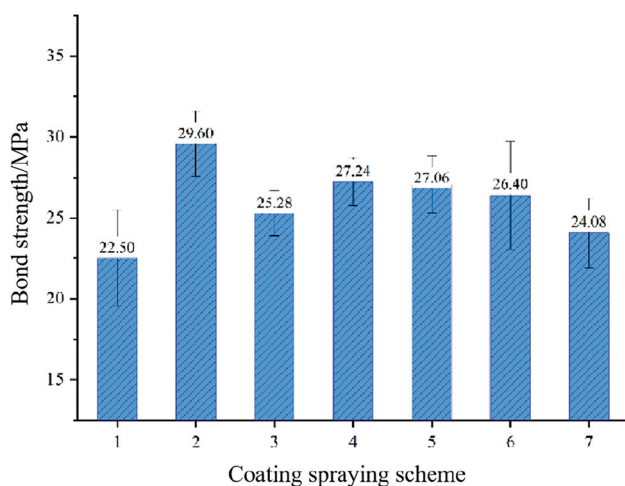
Fig. 3 Bond strength test results of Al_2O_3-PF composite coatings deposited under different spraying schemes

Al_2O_3 powder). It was found that the temperature of Al_2O_3 jet decreased to a certain extent (by about 48.1 °C from 2914.8 to 2866.7 °C) with the increase in the Ar flow rate, while the particle flight velocity increased significantly (by about 43.6 m/s from 449.1 to 492.7 m/s), greatly shortening the heating time of particles in the jet.

It is worth noting that the influences of Ar flow rate changes on Al_2O_3-PF composite powder were also significant. When the Ar flow rate was lower, the morphology of Al_2O_3-PF composite powder entering the jet (a "sandstorm-like" shape) was greatly different from that when the Ar flow rate was higher, as shown in Fig. 6. Moreover, since the outer Al_2O_3 shell is required for heat transfer of Al_2O_3-PF composite powder, higher particle flight velocity is not always better.

1. Coating structure analysis at an Ar flow rate of 50 L/min—Scheme 1

The tensile fracture morphology of composite coatings at an Ar flow rate of 50 L/min is displayed in Fig. 7-1-a and 1-b. An ablated area could be observed obviously in Fig. 1-a, which was considered to be caused by too long retention time of Al_2O_3-PF composite powder in high-temperature jet, and adherence of high-temperature Al_2O_3 molten drops to the coating surface.
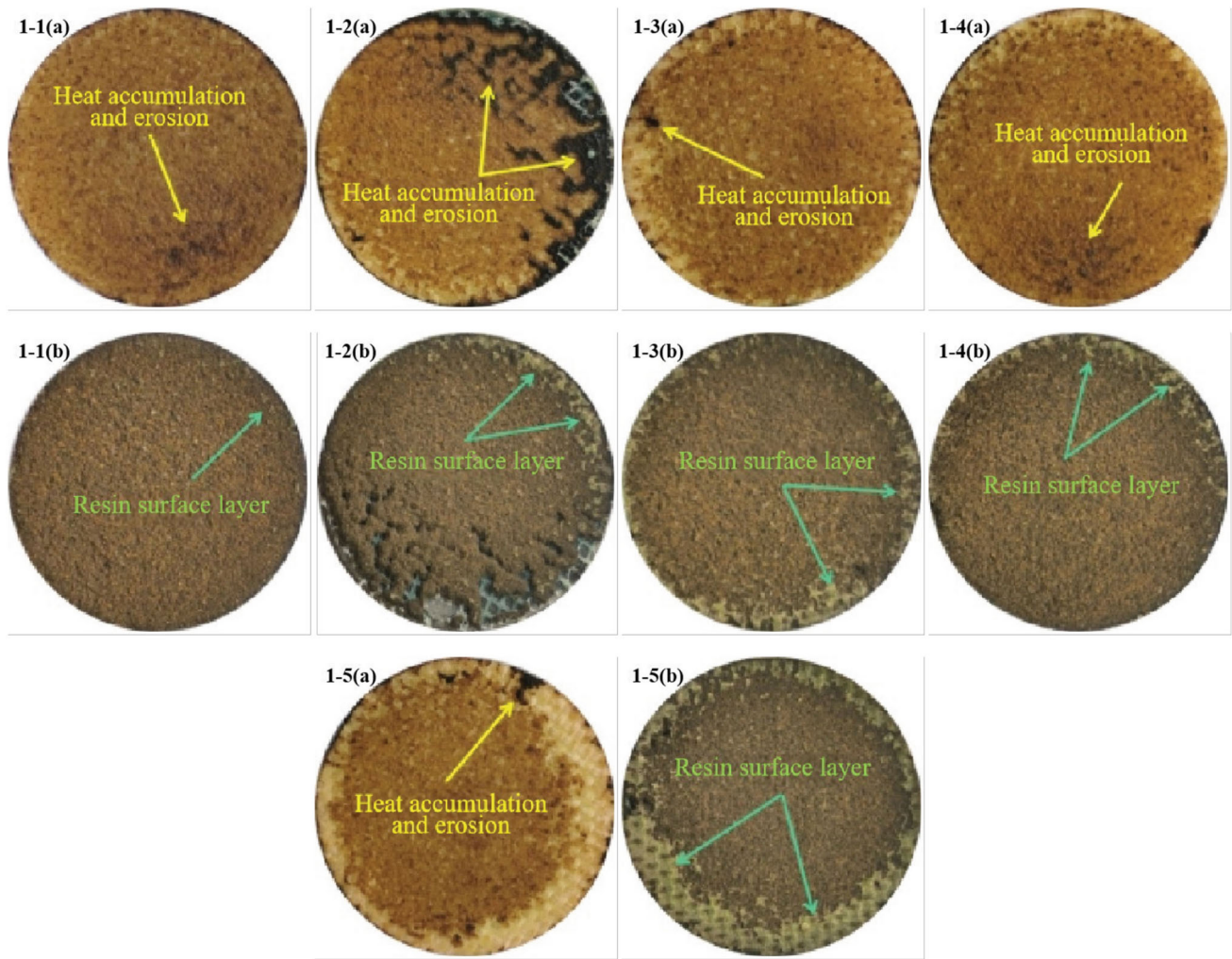
Fig. 4 The cross-sectional morphology and ablation area of the 5 coating samples deposited under spraying Scheme 1 after stretching: (a) all represent the substrate side; (b) all indicate coating side
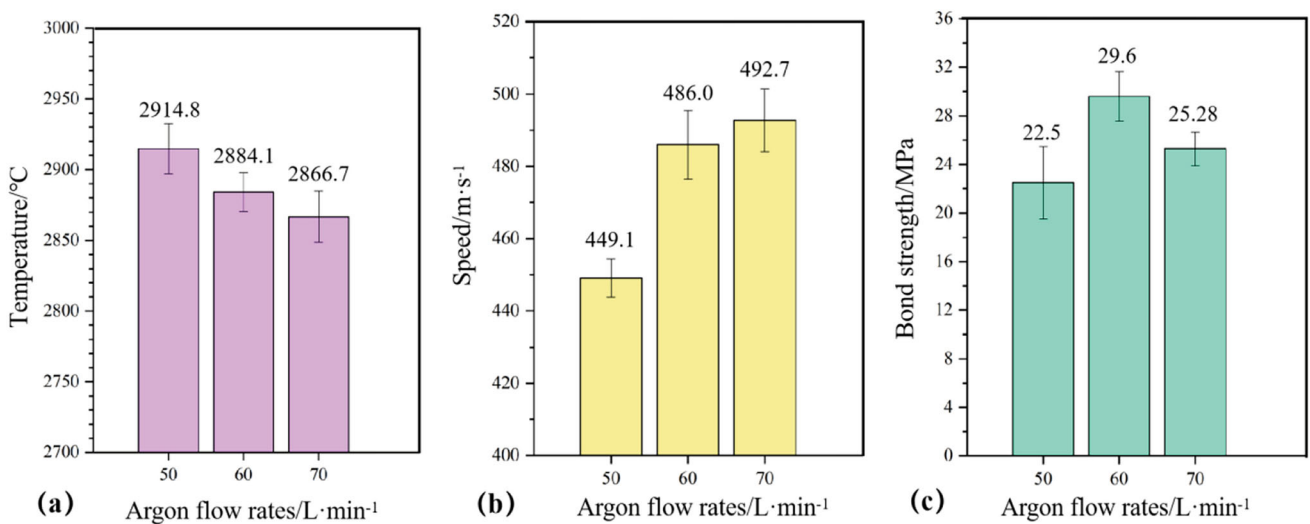
Fig. 5 Effect of argon gas flow rate on particle flight characteristics and coating bonding strength

Meanwhile, the shot blasting cleaning effect of unmelted spherical pure Al_2O_3 powder was not significant due to its low flight velocity, so many large-size pores were left in the coating, as shown in Fig. 8.

Only a small portion of reinforced fiber was exposed in Fig. 8c, suggesting that the sample was fractured mainly in the interior of the composite coating. In Fig. 8d, many unmelted irregular Al_2O_3 particles were found on the coating fracture surface, which could be attributed to the deposition of Al_2O_3-PF composite powder (Ref 20), and these Al_2O_3 particles were uniformly distributed in the coating (Fig. 8b).

2. Coating structure analysis at an Ar flow rate of 60 L/min—Scheme 2

The composite coating deposited in Scheme 2 is displayed in Fig. 9. As can be seen from the cross-sectional morphology (Fig. 9a, b), there were pores in the coating but they were uniformly distributed in the coating, and no obvious molten Al_2O_3 block and unmelted spherical pure Al_2O_3 powder were found in the pores. Therefore, the pores in the coating in Scheme 2 may primarily come from the overflow of gas released by polycondensation reaction of heated PF and gas involved in the spraying process (Ref 10-14).

Analysis suggests that when the Ar flow rate increases to 60 L/min, the flight velocity of spherical pure Al_2O_3 powder rises, the shot blasting effect becomes more significant, and the particles with a poor deposition effect during spraying are removed, making the coating structure more compact. Besides, with the increase in the flight velocity of Al_2O_3-PF composite powder, the heating of particles is weakened, so the excessive aggregation and accumulation of unmelted Al_2O_3 particles in composite powders can be avoided after impinging the matrix. In Fig. 9d, the content of aggregated Al_2O_3 particles in the coating fracture section greatly declined, and PF was obviously visible at the fracture section, indicating that the unmelted Al_2O_3 particles in the coating are bonded by PF. Therefore, the flight velocity of Al_2O_3 and PF particles increases and their temperature decreases slightly when the Ar flow rate is 60 L/min, achieving a good match between velocity and temperature.

3. Coating structure analysis at an Ar flow rate of 70 L/min—Scheme 3

When the Ar flow rate increases to 70 L/min, many pores and molten Al_2O_3 blocks could be clearly observed in the coating (Fig. 10), and the pores were mainly distributed at the coating-matrix bonding position. As shown in Fig. 10c, d, no resin matrix structure was found at the tensile fracture section of the coating, so the fracture was mainly located in the interior of the composite coating.

There are two main reasons: First, the increase in particle flight velocity of Al_2O_3-PF composite powder leads to insufficient heat transfer of composite powder, making it easy to form a second kind of flake morphology (Ref 20), thus resulting in massive aggregation of unmelted Al_2O_3 particles in composite powder (Fig. 10b). Second, spherical pure Al_2O_3 powder has high temperature and high velocity, so the high-temperature particles are more likely to remain in the coating. As a result, PF around the high-temperature particles will be persistently heated and undergo a strong polycondensation reaction, ultimately forming many pores. In addition, high temperature and high velocity contribute to the deposition of Al_2O_3 in coatings, so many molten Al_2O_3 blocks emerge locally in coatings, resulting in PF ablation in coatings.
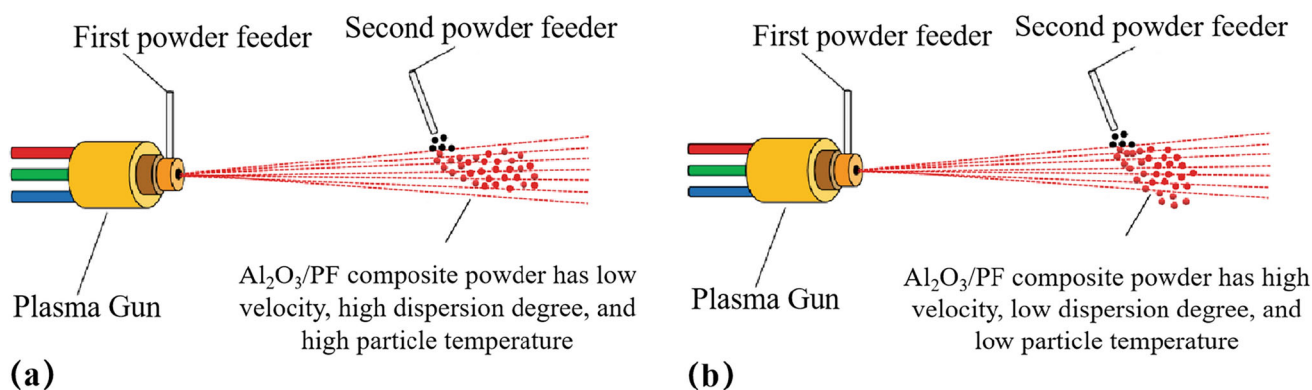

Fig. 6 The effect of argon gas flow rate on Al_2O_3/PF composite powder: (a) the argon gas flow rate is 50 L/min; (b) argon gas flow rate is 70 L/min
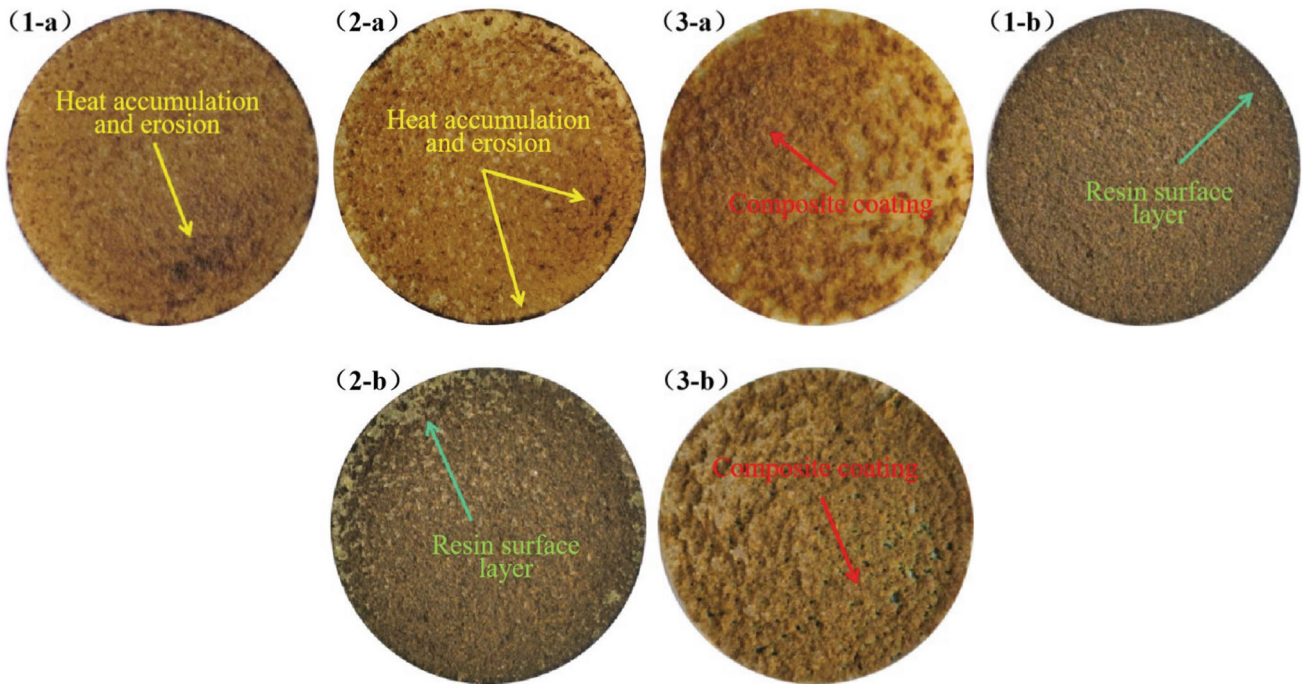
Fig. 7 The cross-sectional morphology and ablation area of the coating samples deposited by spraying Schemes 1, 2, and 3 after stretching: (a) all represent the substrate side; (b) all indicate coating side

Fig. 8 Scheme 1 coating sample cross section and tensile cross section: (a-b) coating cross-sectional morphology; (c-d) tensile cross-sectional morphology
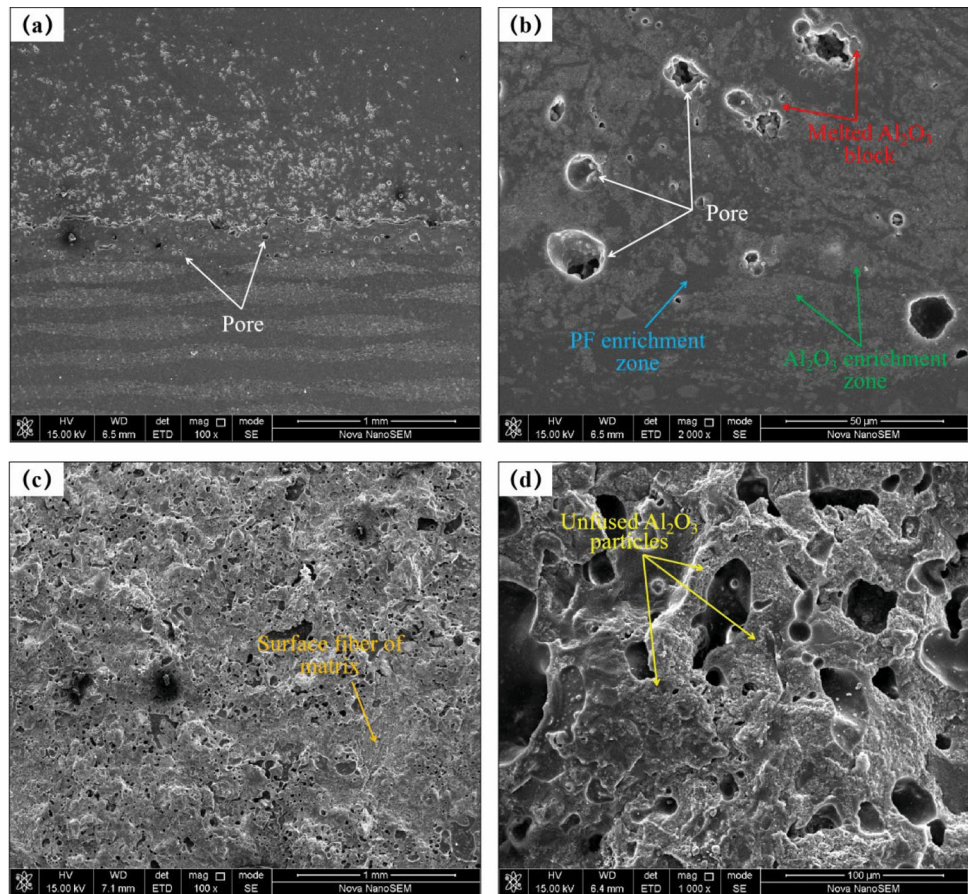
Fig. 9 Cross section and tensile section of coating sample in Scheme 2: (a-b) Cross-sectional morphology of the coating; (c-d) tensile cross-sectional morphology
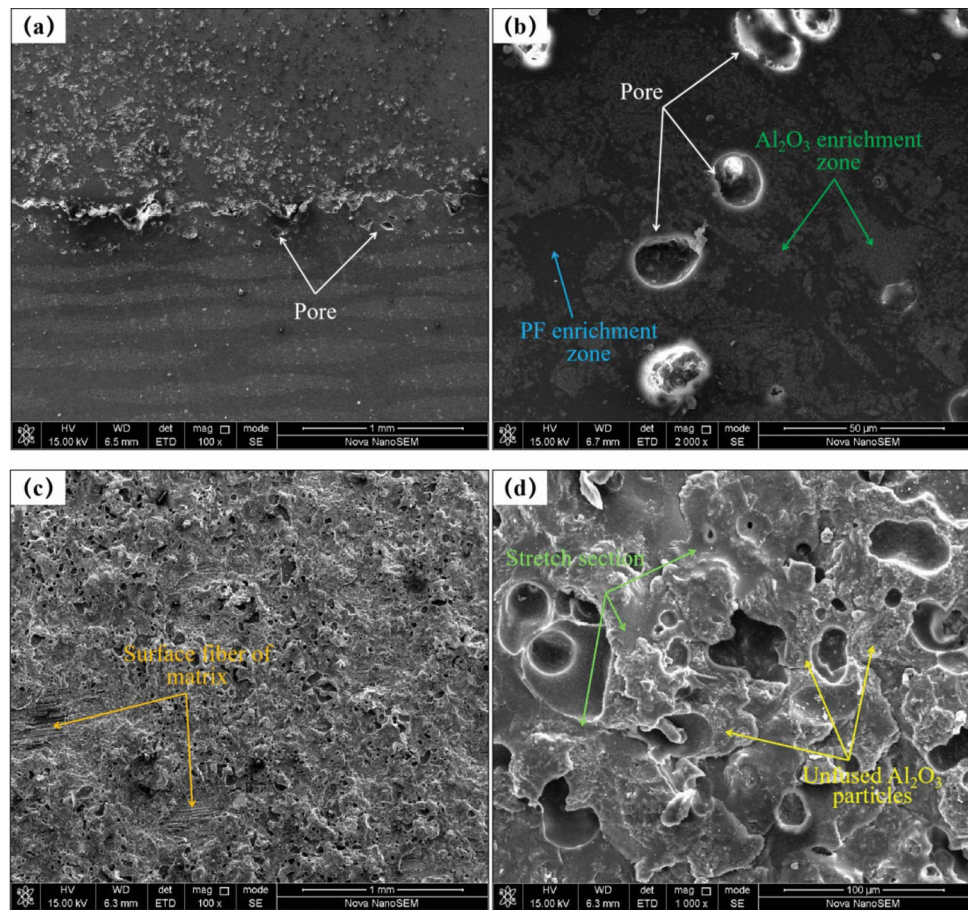
Influences of Spraying Voltage (V)

In the experiment exploring the influence of spraying voltage, the highest spraying voltage was set to 115 V, because it was found in the preliminary investigations that the spraying voltage > 115 V had approached the maximum withstand voltage of the anode nozzle, which led to spraying voltage instability and equipment damage.

The influence rule of spraying voltage on the temperature and velocity of spherical pure Al_2O_3 powder jet and on the bonding strength of composite coating is displayed in Fig. 11. It was found that the temperature (an increase by about 211.8 °C from 2772.6 to 2984.4 °C) and velocity (an increase by about 34.2 m/s from 476.4 to 510.6 m/s) of spherical pure Al_2O_3 powder jet significantly rose with the increase in spraying voltage from 105 to 115 V.

Meanwhile, the rate of temperature change of particles was higher than that of velocity change. There are two major reasons: First, after the spraying voltage increased, both spraying power and enthalpy of plasma arc increased rapidly, thus effectively increasing the jet temperature. Second, the amount of H_2 added to change the voltage was as small as about 3–5 L/min, so the change in total gas flow had little influence on the particle flight velocity.

Under normal conditions, a higher temperature of spray particles corresponds to more thorough melting, and a higher velocity produces stronger kinetic energy, so the particles spread out more fully when impinging the matrix, yielding a more compact structure and better properties of the coating. However, according to the analysis results of the influences of Ar flow rate on coatings in "Influences of Ar flow rate (L·min-1)" Section, excessive heat input during spraying was not conducive to coating deposition, and a sharp increase in the heat would cause resin ablation in the matrix and coating, as shown in Fig. 12.

In Fig. 12, the spraying voltage was only increased from 105 to 115 V in Schemes 2, 4 and 5, but the coating structure had greatly changed. Specifically, only a very small ablated area is seen in Fig. 2-a, the overall coating structure was intact in Fig. 2-b, and severe ablation occurred in Fig. 4-a and 5-a and was mainly located in the composite coating. It can be inferred that persistent heat accumulation in the spraying process caused PF ablation in the composite coating, leading to coating fracture in Fig. 4-b and 5-b. To sum up, PF ablation causes structural degradation of the composite coating and reduces the cohesive strength of the coating.

Fig. 10 Cross section and tensile section of coating sample in Scheme 3: (a-b) cross-sectional morphology of the coating; (c-d) tensile cross-sectional morphology
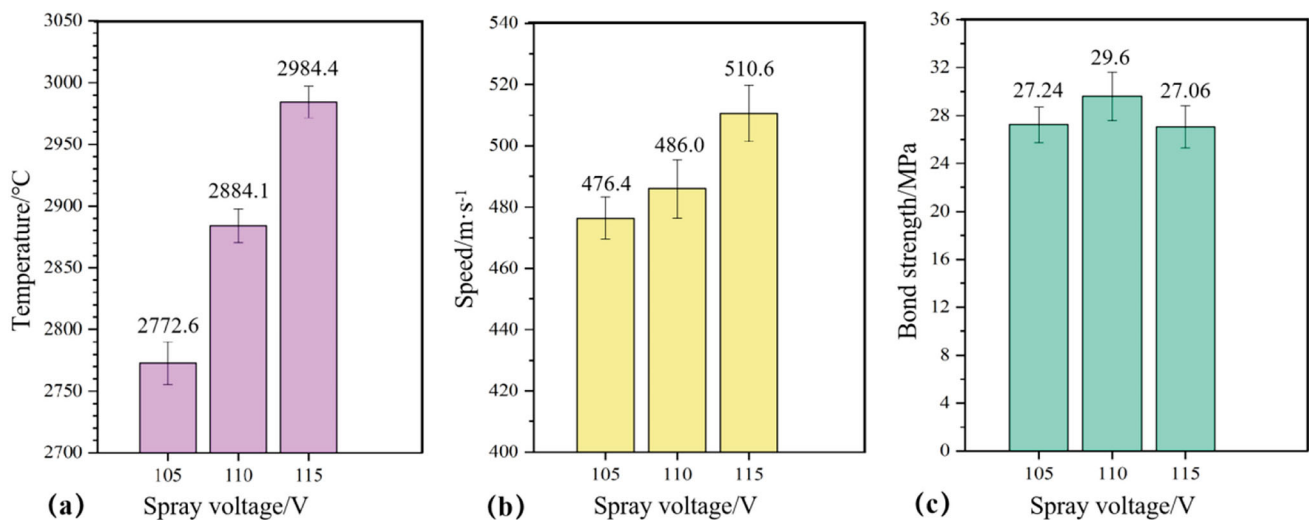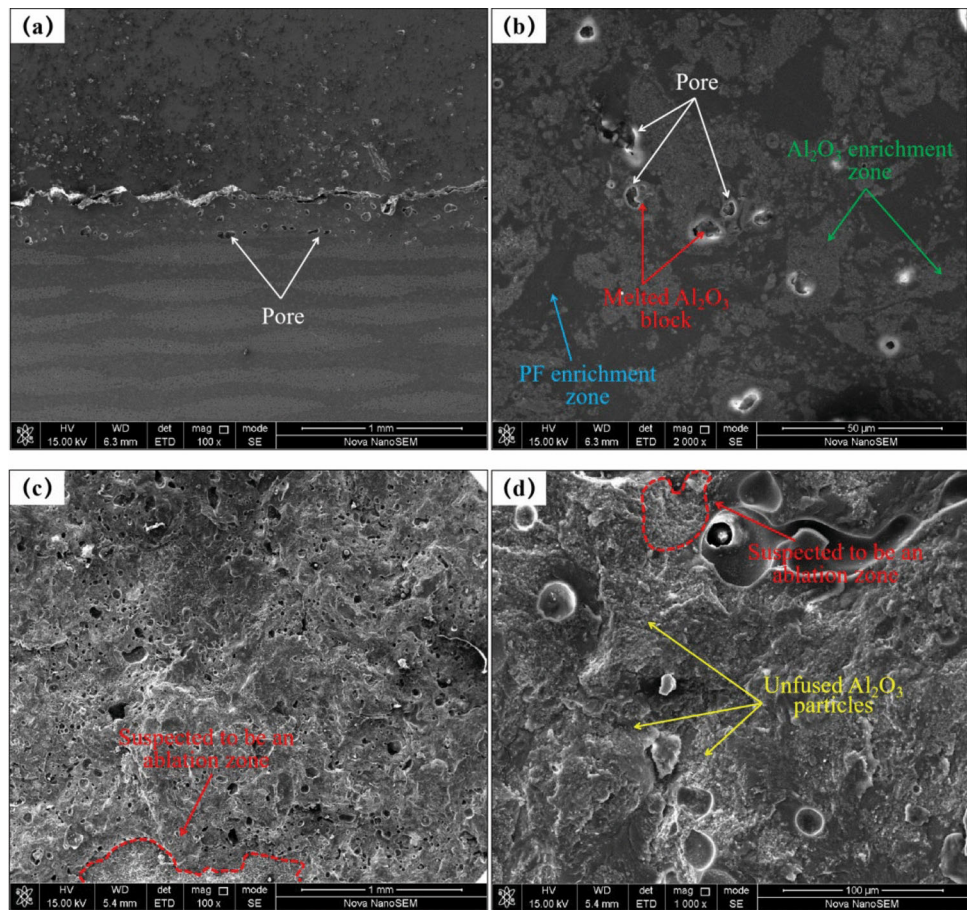

Fig. 11 Effect of spray voltage on particle flight characteristics and coating bonding strength

1. Coating structure analysis at a spraying voltage of 105 V—Scheme 4

Combined with the melting deposition behavior of Al_2O_3 and PF powders and the coating deposition mechanism (Ref 20), analysis suggests that when the spraying voltage is 105 V, severe ablation of the polymer resin in the composite coating can be attributed to "high-temperature and low-velocity" molten drops.

As the coating morphology in Figure 12-4-a and 4-b shows, PF in the coating was mainly ablated by "high-temperature and low-velocity" Al_2O_3 particles (only a
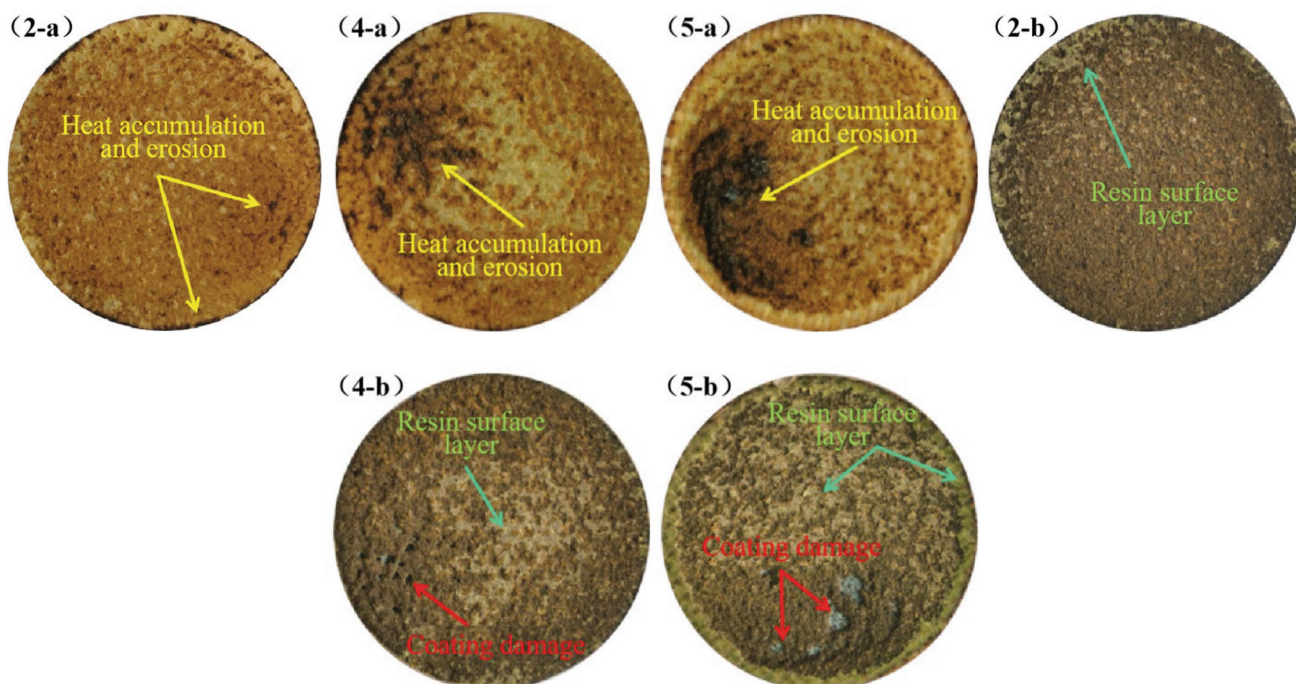
Fig. 12 The cross-sectional morphology and ablation area of the coating samples deposited by spraying Schemes 2, 4, and 5 after stretching: (a) all represent the substrate side; (b) all indicate coating side

small portion of matrix resin is observed in Fig. 4-b, indicating that damage was caused to the composite coating structure in Scheme 4). The jet temperature was the lowest when the spraying voltage was 105 V, but it was still as high as 2772.6 °C, far higher than the thermal decomposition temperature of the resin material, so it was inevitable to locally ablate PF in the matrix resin or coating. Besides, the particles were less capable of washing the ablated area due to low flight velocity, so the ablated area continuously endured and accumulated heat in the subsequent spraying process, and the ablation products also remained and accumulated in the coating, ultimately affecting the structure and properties of the coating.

It was observed that there were a large number of pores at the coating-matrix bonding position (Fig. 13a), seriously reducing the coating-matrix bonding strength. As analyzed from Fig. 13b, there were mainly two types of pores: coarse pores formed by melted and semi-melted high-temperature Al_2O_3 particles ablating PF and regular pores formed by the overflow of gas involved in the spraying process and gas released by the chemical reaction of PF.

Furthermore, the tensile fracture morphology of the coating was analyzed. The results revealed that the areas indicated by the red dotted lines in Fig. 13c were all aggregates of unmelted Al_2O_3 particles, and they differed greatly from similar morphologies in Fig. 9. In Fig. 13c, many fine particles were observed in the aggregates of unmelted Al_2O_3 particles, and PF was hardly seen as an

"adhesive", suggesting that PF ablation had occurred in this area, thus resulting in a lower bonding strength in this area. In Fig. 13d, ablated holes formed by high-temperature molten Al_2O_3 blocks could be observed.

2. Coating structure analysis at a spraying voltage of 110 V—Scheme 2

Figure 14 displays the cross-sectional morphology and tensile fracture morphology of composite coatings deposited at a spraying voltage of 110 V. It was found that the overall morphology of the coating was good, the pores were evenly distributed in the coating, and only a small number of molten Al_2O_3 blocks were present in the coating, reducing the ablation damage to the coating. The pores in the coating mainly came from the overflow of gas (such as H_2O and CO_2) released by polycondensation reaction of PF and gas involved in the spraying process. Meanwhile, PF uniformly filled the pores among unmelted Al_2O_3 particles, which acted as an adhesive.

The tensile fracture morphology of coatings was further observed (Fig. 14c, d). No large-area aggregation of unmelted Al_2O_3 particles was found at the tensile fracture section of the coating, but PF uniformly wrapped and filled unmelted Al_2O_3 particles. Meanwhile, unmelted spherical pure Al_2O_3 powder was observed, suggesting that the heat-melting effect on spherical pure Al_2O_3 powder was weakened when Scheme 2 was adopted. Therefore, a good shot blasting effect was achieved while reducing PF ablation in the coating.

Fig. 13 Cross section and tensile section of coating sample in Scheme 4: (a-b) cross-sectional morphology of the coating; (c-d) tensile cross-sectional morphology
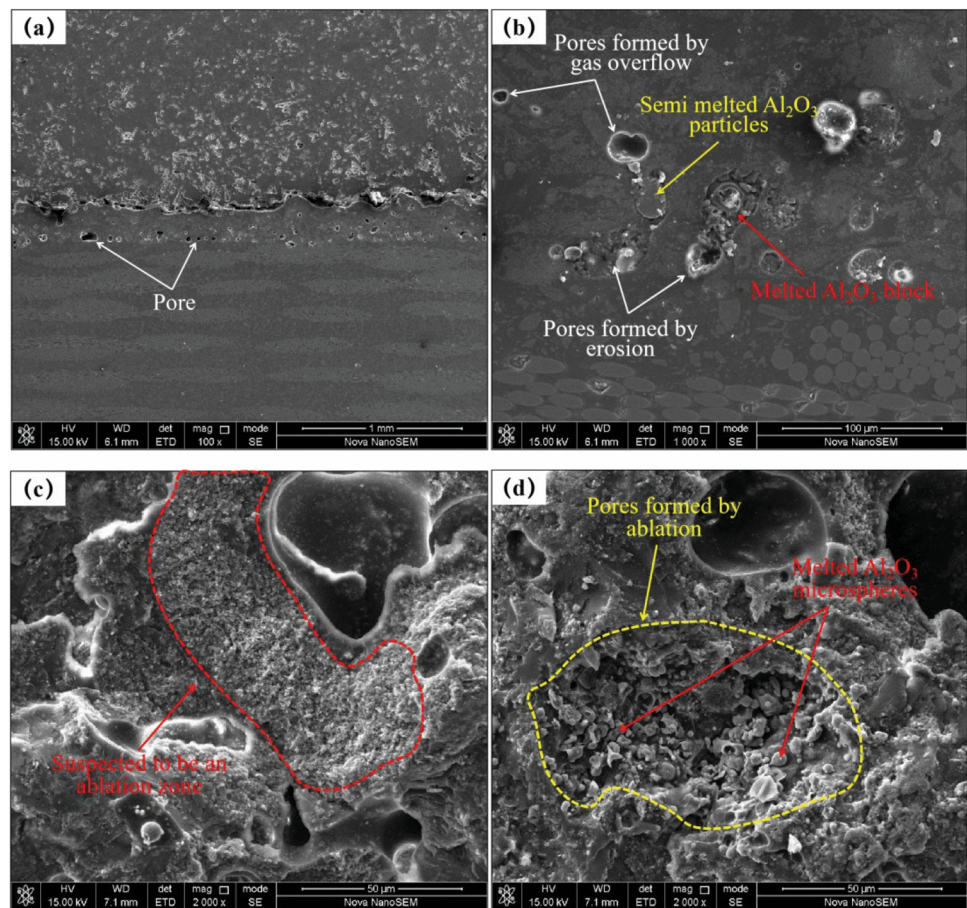
3. Coating structure analysis at a spraying voltage of 115 V—Scheme 5

The macroscopic morphologies were compared between Figure 12-5-a and 5-b, and severe ablation was found in the composite coating, suggesting that severe ablation was caused to the coating in Scheme 5. Analysis suggests that ablation of the polymer resin in Scheme 5 can be attributed to "high-temperature and high-velocity" molten drops.

Figure 15 displays the cross-sectional morphology and tensile fracture morphology of composite coatings deposited at a spraying voltage of 115 V. Many pores were found in the composite coating, but they were mainly distributed in the interior of the coating as compared to those at a spraying voltage of 105 V. Meanwhile, a large number of molten Al_2O_3 blocks and ablated holes in the coating and pores in molten Al_2O_3 blocks were observed.

At the tensile fracture section of the coating (Fig. 15c, d), it could be clearly observed that molten Al_2O_3 blocks existed in the coating in an independent form and had no close bonding with the coating. Meanwhile, a poor overlapping state of molten Al_2O_3 blocks could be observed, with many pores and cracks inside, which would seriously affect the cohesive strength of the composite coating.

Analysis shows that the H_2 flow was added to increase the spraying voltage, so the total gas flow rose and the flight velocity of Al_2O_3 particles increased simultaneously, making it easier for Al_2O_3 particles to be embedded in the coating. Moreover, the temperature of Al_2O_3 powder jet increased by about 211.8 °C with the increase in spraying voltage. As a result, the polymer resin in the matrix or coating was ablated instantaneously due to the sharp temperature rise, and the accumulation of more heat led to the delamination of matrix resin and fiber layer.

Influences of Spraying Current (A)

When the nozzle structure is fixed, increasing the spraying current can effectively improve the efficiency of arc ionization of gas between the cathode and the anode, so that the plasma will expand rapidly, thus increasing the temperature and velocity of plasma jet.

The changes in temperature and velocity of spherical pure Al_2O_3 powder jet as a function of spraying current are shown in Fig. 16. It was found that with the increase in spraying current, the jet temperature rose by about 94.3 °C from 2869.3 to 2963.6 °C, and the jet velocity rose by about 44 m/s from 476.8 to 520.8 m/s. Moreover, when the

Fig. 14 Cross section and tensile section of coating sample in Scheme 2: (a-b) cross-sectional morphology of the coating; (c-d) tensile cross-sectional morphology
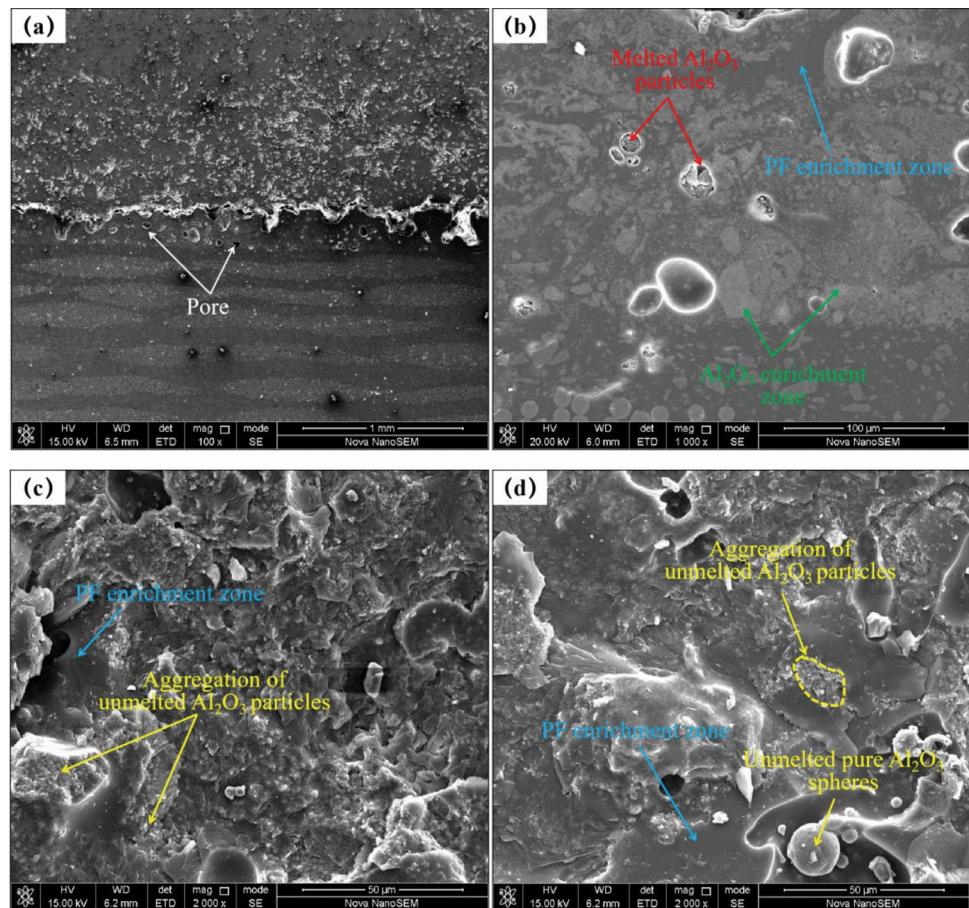
spraying current increased from 400 to 410 A, the rates of jet temperature and velocity changes were significantly lower than those when the spraying current increased from 410 to 420 A. It can be inferred that the increase in spraying current (increase in spraying power) has a great influence on the melting and flight states of spray powder.

What is noteworthy is that when the spraying current increased from 410 to 420 A, the molecular structure of the resin material would be destroyed by the continuous heat accumulation despite small changes in the Al_2O_3 jet temperature (an increase by about 79.5 °C). In actual spraying, due to an extremely low coating ratio of spherical pure Al_2O_3 powder and the need to control the matrix temperature by cooling, the preparation of one group of samples requires about 50-60 min, during which the heat accumulation generated cannot be ignored.

The tensile fracture morphology of coatings was compared with spraying current as a single variable in Fig. 17. Severe ablation was found in both Scheme 6 and Scheme 7. Two possible ablation mechanisms in the spraying process were summarized in the analysis of the influences of spraying voltage. It was found that the influence rule of spraying current on jet temperature and velocity was basically consistent with that of spraying voltage (Fig. 11

and 16). Therefore, it was considered that the ablation in Scheme 6 and Scheme 7 was still attributed to "high-temperature and low-velocity molten drops" and "high-temperature and high-velocity molten drops".

1. Coating structure analysis at a spraying current of 400 A—Scheme 6

The cross-sectional morphology and tensile fracture morphology of composite coatings prepared at a spraying current of 400 A are shown in Fig. 18. It could be found that the pores of the coating were mainly distributed in the interior of the coating, rather than limited to the coating-matrix bonding position. The reason is that the particle temperature in Scheme 6 (jet temperature: 2869.3 °C) was higher than that in Scheme 4 (jet temperature: 2772.6 °C), so the high-temperature particles were more likely to cause PF ablation and holes in the coating.

In addition, the tensile fracture section of the coating (Fig. 18c, d) was almost full of pores large in both size and number. It can be inferred that the coating structure is loose due to the presence of a lot of pores in the composite coating, so fracture occurs along the pore section under tensile force.

Fig. 15 Cross section and tensile section of Scheme 5 coating sample: (a-b) cross-sectional morphology of the coating; (c-d) tensile cross-sectional morphology
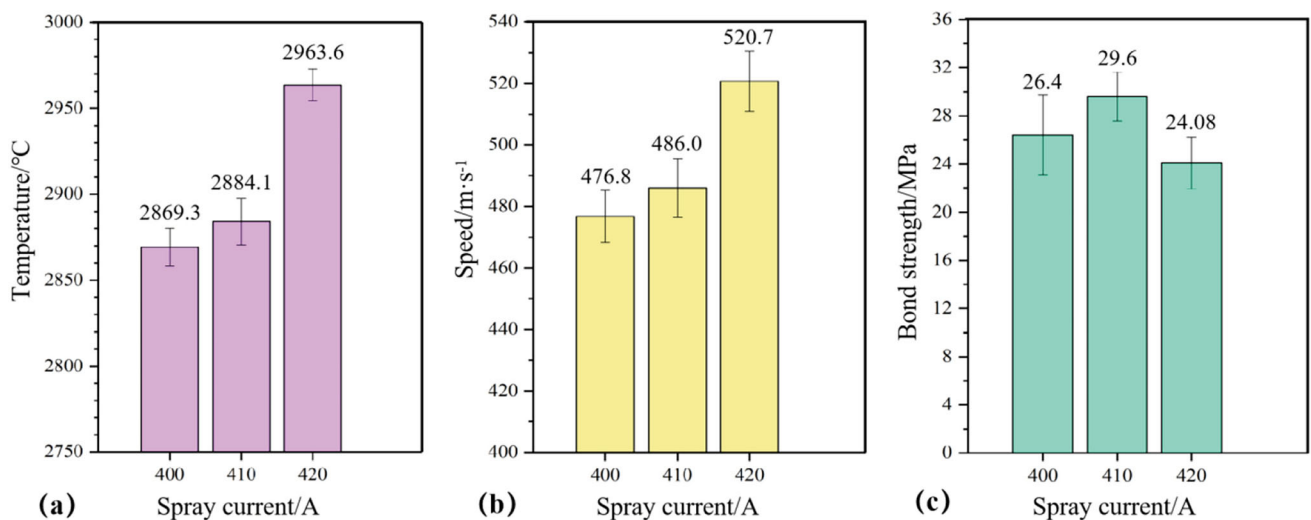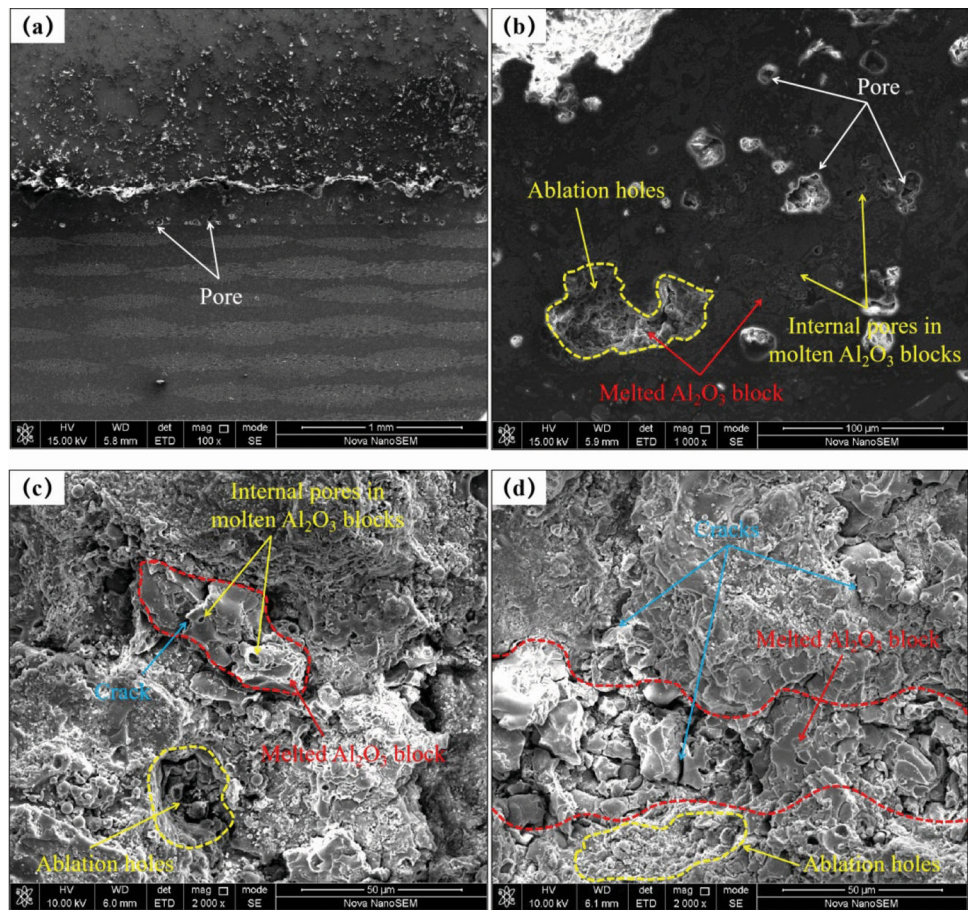
Fig. 16 Effect of spray current on particle flight characteristics and coating bonding strength
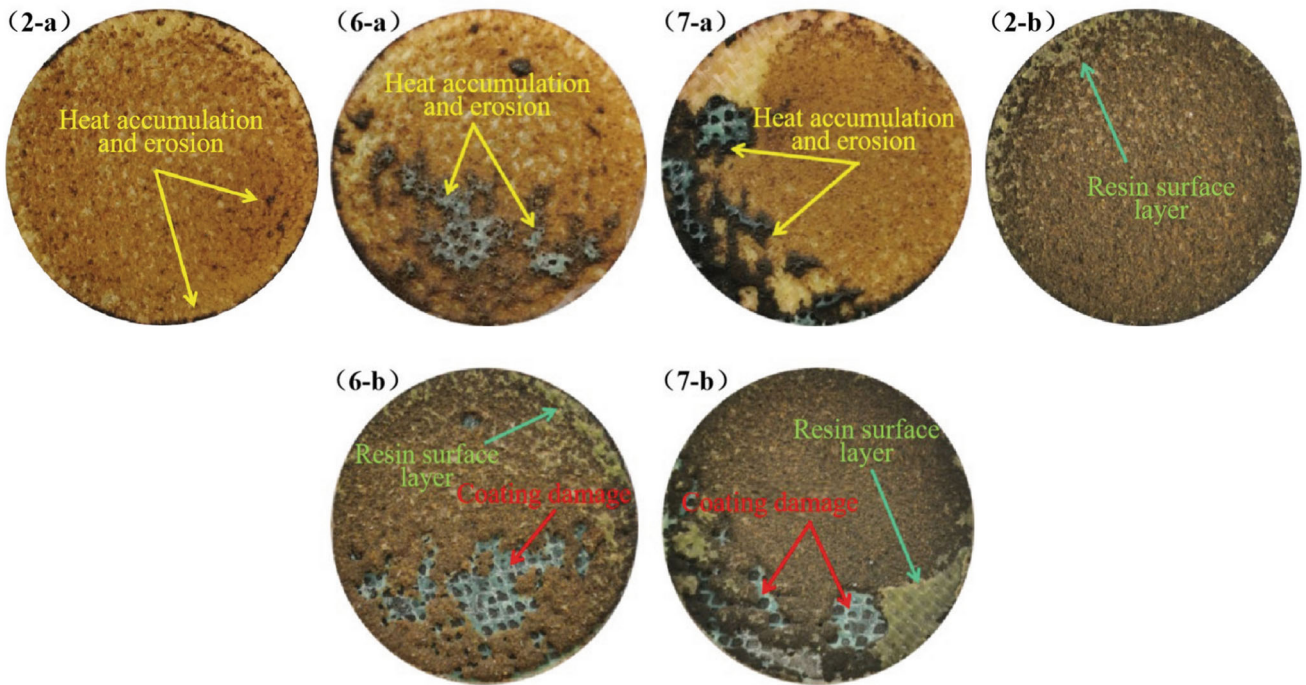
2. Coating structure analysis at a spraying current of 410 A—Scheme 2

The cross-sectional morphology and tensile fracture morphology of composite coatings prepared in Scheme 2 are displayed in Fig. 14. It could be clearly seen that the size and number of pores in the coating obviously declined, without a large number of molten Al_2O_3 blocks or obvious ablated holes in the coating.

From Fig. 16, analysis suggests that when the spraying current is 410 A, the influences of heat accumulation on the

Fig. 17 The cross-sectional morphology and ablation area of the coating samples deposited by spraying Schemes 2, 6, and 7 after stretching: (a) All represent the substrate side; (b) All indicate coating side

Fig. 18 Cross section and tensile section of coating sample in Scheme 6: (a-b) cross-sectional morphology of the coating; (c-d) tensile cross-sectional morphology
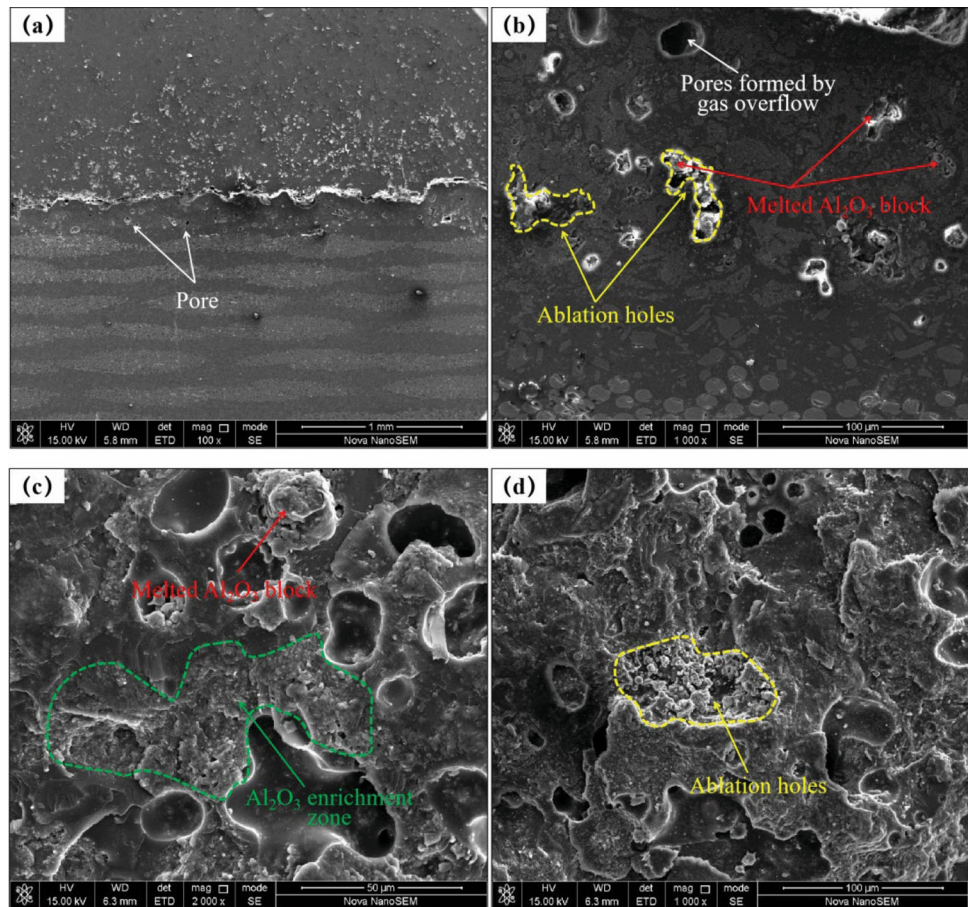
matrix and coating during spraying can be alleviated to a certain extent, enhancing the overall properties of the coating.

3. Coating structure analysis at a spraying current of 420 A—Scheme 7

Figure 19 shows the cross-sectional morphology and tensile fracture morphology of composite coatings deposited at a spraying current of 420 A. It was found that there were a large number of pores in the coating, and the structure of the composite coating was loose. Due to the ablation effect of high-temperature particles, a lot of ablated holes were produced in the coating. Furthermore, the particle flight velocity was greatly increased (up to 520.8 m/s) by increasing the spraying current, so aggregation (Fig. 19b, c) and clustered distribution of Al_2O_3 particles in Al_2O_3-PF composite powder were more frequently seen in the coating. As a result, PF failed to fully bond and fill the pores among Al_2O_3 particles, reducing the bonding strength of the coating.

To sum up, the influences of Ar flow rate, spraying voltage and spraying current on the melting and deposition behavior of Al_2O_3 and PF powders during the spraying of Al_2O_3-PF composite coatings are summarized and compared in Table 9, further explaining and validating the reliability of the optimal spraying process optimized through orthogonal tests in the preparation of composite coatings.

In addition, by comparison with the previously prepared Al_2O_3-PF composite coatings (Ref 20), the following benefits of the optimized spraying process on the deposition of composite coatings were found:

1. The content of Al_2O_3 in the composite coating was further increased as compared to that before optimization, especially the content of molten Al_2O_3 blocks, which was beneficial to improving the ablation and wear resistance of the composite coating.

2. The ablation of molten Al_2O_3 blocks against the coating was effectively controlled, few defects such as pores in the composite coating occurred, and melted PF could fully fill the pores among Al_2O_3 particles, making the coating more compact.

3. The thermal damage to the polymer matrix during the spraying was significantly undermined after process optimization. In terms of the cross-sectional morphology of the matrix before and after optimization, it was clearly found that the surface delamination of the resin

Fig. 19 Cross section and tensile section of Scheme 7 coating sample: (a-b) cross-sectional morphology of the coating; (c-d) tensile cross-sectional morphology
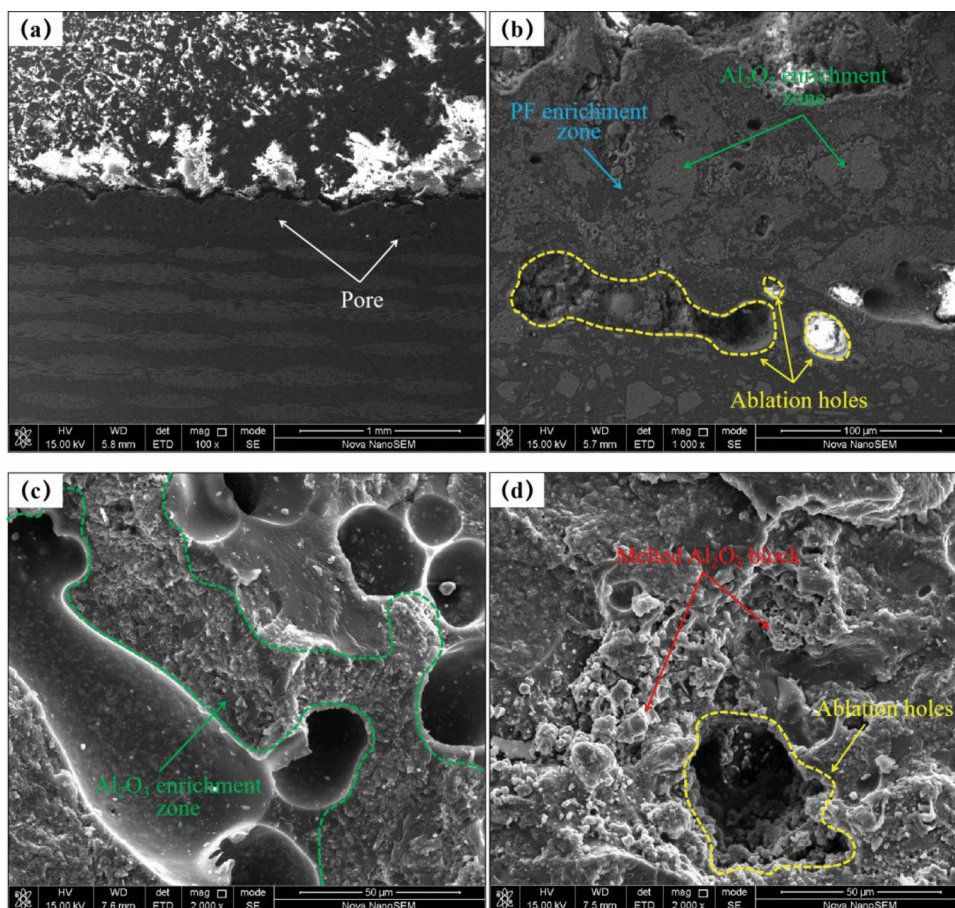
Table 9 The influence mechanism of various experimental factors on the deposition of composite coatings

Experimental factors		The impact mechanism on coating deposition
Argon gas flow rate	50L min^{-1}	① The flying speed of spherical pure Al_2O_3 powder is low, and the effects of shot peening and erosion are weak; ② The Al_2O_3-PF composite powder has a high degree of dispersion in the jet; ③ Severe coating erosion
	60L min^{-1}	① The speed and temperature of the two powders are reasonably matched, and the shot peening effect of spherical pure Al_2O_3 powder is significant
	70L min^{-1}	① An increase in Al_2O_3 frits results in severe coating erosion; ② The Al_2O_3-PF composite powder is prone to form a second type of spreading, leading to an increase in the aggregation degree of Al_2O_3 particles
Spray voltage	105 V	① Spherical pure Al_2O_3 powder is prone to form "high-temperature and low-speed" droplets, resulting in severe coating erosion; ② The shot peening and scouring effects of spherical pure Al_2O_3 powder are weak
	110 V	① The speed and temperature of the two powders are reasonably matched, and the shot peening and flushing effects of spherical pure Al_2O_3 powder are obvious
	115 V	① Spherical pure Al_2O_3 powder is prone to form "high-temperature and high-speed" droplets, resulting in severe coating erosion; ② Heat accumulation leads to interlayer cracks in the resin matrix
Spray current	400 A	① Low spraying power, spherical pure Al_2O_3 powder is prone to form "high-temperature and low-speed" droplet ablation coatings; ② Increase in coating porosity
	410 A	① The speed and temperature of the two powders are reasonably matched, and the shot peening and flushing effects of spherical pure Al_2O_3 powder are obvious
	420 A	① High spraying power, spherical pure Al_2O_3 powder is prone to form "high-temperature and high-speed" droplet ablation coatings; ② The porosity of the coating increases; ② The Al_2O_3-PF composite powder is prone to form a second type of spreading, leading to an increase in the aggregation degree of Al_2O_3 particles

matrix occurred in the spraying process before optimization. However, no delamination of the matrix was observed after optimization, effectively avoiding the matrix damage caused by long-term heat accumulation in the spraying process. It is believed that this is one of the important reasons for the improved bonding strength of composite coatings.

Conclusions

This article determines the main and secondary factors of using supersonic high-energy plasma spraying Al_2O_3-PF composite coating on the surface of polymer matrix composite materials (glass fiber-reinforced epoxy resin) through the design of a four-factor three-level orthogonal experiment. The spraying voltage, Ar flow rate, and spraying current have a significant impact on the experimental results and are the main influencing factors; The second powder feeding position has a relatively small impact on the experimental results and is a secondary influencing factor. The optimal process for coating preparation is: Ar flow rate of 60 L/min, spraying voltage of 110 V, spraying current of 410 A, and second powder feeding position of 60 mm. The deposited composite

coating has good structural density, and the average bonding strength of the coating can reach 29.60 MPa.

Furthermore, the influences of Ar flow rate, spraying voltage and spraying current on the deposition process of Al_2O_3-PF composite coatings were discussed and analyzed by single-factor tests.

1. The Ar flow rate exerted an influence on composite coatings by changing the particle flight velocity. With the changes in the Ar flow rate, the flight velocity of Al_2O_3 and PF powders changed sharply, which further affected their state and effect during deposition.

2. The spraying voltage exerted an influence on composite coatings by changing the particle temperature, and with the increase in spraying voltage, the particle temperature rose sharply, causing more severe ablation. In addition, the changes in spraying voltage would also influence the particle flight velocity to some extent. Combined with the changes in particle velocity and temperature, ablation that occurred in the spraying process could be attributed to "high-temperature and low-velocity" molten drops and "high-temperature and high-velocity" molten drops.

3. Spraying current mainly influenced the efficiency of arc ionization of gas between the cathode and the anode, thus affecting the temperature and velocity of plasma jet. Therefore, the influences of spraying

current on the deposition of composite coatings were almost the same but slightly less than those of spraying voltage.

References

1. K. Agarwal, S.K. Kuchipudi, B. Girard et al., Mechanical Properties of Fiber Reinforced Polymer Composites: A Comparative Study of Conventional and Additive Manufacturing Methods, *J. Compos. Mater.*, 2018, **52**(23), p 3173-3181.

2. M.Z. Rahman, K. Jayaraman, and B.R. Mace, Influence of Damping on the Bending and Twisting Modes of Flax Fibre-Reinforced Polypropylene Composite, *Fibers Polym.*, 2018, **19**, p 375-382.

3. X. Tang and X. Yan, A Review on the Damping Properties of Fiber Reinforced Polymer Composites, *J. Ind. Text.*, 2020, **49**(6), p 693–721.

4. H.L. Li, S.S. Yao et al., Research Progress of Epoxy Resin/Carbon Fiber Thermal Conductive Composite, *J. Jilin Inst. Chem. Technol.*, 2020, **37**(11), p 28-32.

5. Z. W. Li, Preparation and Properties of Polymer-Based Composites with High Thermal Conductivity. Harbin: Harbin institute of technology, 2015

6. L. Yu and T.X. Wang, Application of Composite Materials in Ship Construction, *Sci. Technol. Innov. Guide*, 2019, **16**(26), p 80-81.

7. S. Sudha and G. Thilagavathi, Analysis of Electrical, Thermal and Compressive Properties of Alkali-Treated Jute Fabric Reinforced Composites, *J. Ind. Text.*, 2018, **47**(6), p 1407-1423.

8. X. Fan, Application Status and Development Trend of Carbon Fiber Composites, *Chem. Ind.*, 2019, **37**(4), p 12-16.

9. Q.Q. Peng, M. Liu, Y.F. Huang et al., Research Status and Prospects of Surface Protective Coatings for Polymer Matrix Composites, *Surf. Technol.*, 2022, **51**(2), p 86-107.

10. M. Ivosevic, R. Knight, S.R. Kalidindi et al., Erosion/oxidation Resistant Coatings for High Temperature Polymer Composites, *High Perform. Polym.*, 2003, **15**(4), p 503-517.

11. M. Ivosevic, R. Knight, S.R. Kalidindi et al., Adhesive/cohesive Properties of Thermally Sprayed Functionally Graded Coatings for Polymer Matrix Composites, *J. Therm. Spray Technol.*, 2005, **14**(1), p 45-51.

12. M. Ivosevic, R. Knight, S.R. Kalidindi et al., Solid Particle Erosion Resistance of Thermally Sprayed Functionally Graded Coatings for Polymer Matrix Composites, *Surf. Coat. Technol.*, 2006, **200**(16–17), p 5145-5151.

13. M. Ivosevic, R. Knight, S.R. Kalidindi, G.R. Palmese, J.K Sutter, Microstructure and Properties of Thermally Sprayed Functionally Graded Coatings for Polymeric Substrates. In: International thermal spray conference and exposition (2003), pp. 212119

14. M. Ivosevic, R. Knight, S.R. Kalidindi et al, Optimal Substrate Preheating Model for Thermal Spray Deposition of Thermosets onto Polymer Matrix Composites. In: International thermal spray conference and exposition (2003)

15. H.L. Tian, C.L. Wang, M.Q. Guo et al., Study on Process and Performance of Thermal Protective Coating on Polyimide Resin Matrix Composite, *Ceram. Int.*, 2020, **46**(8), p 12744-12758.

16. M.H. Guo, A.G. Liu et al., Analysis of Protective Performance of Ceramic Coating for Resin Matrix Composites, *Trans. China Weld. Inst.*, 2005, **26**(11), p 13-16.

17. Y.L. Zhang, M.H. Guo, A.G. Liu et al., Preparation of Lightweight Ceramic Coating for High Temperature Resin Matrix Composites, *Trans. China Weld. Inst.*, 2005, **026**(003), p 5-8.

18. A.G. Liu, M.H. Guo, M.H. Zhao et al., Arc Sprayed Erosion-Resistant Coating for Carbon Fiber Reinforced Polymer Matrix Composite Substrates, *Surf. Coat. Technol.*, 2006, **200**(9), p 3073–3077.

19. K. Miyoshi, J.K. Sutter, R.J. Mondry et al., Measurements of Erosion Wear Volume Loss on Bare and Coated Polymer Matrix Composites, *Berliner und münchener tierrztliche wochenschrift*, 2003, **94**(22), p 445-448.

20. Q.Q. Peng, M. Liu, Y.F. Huang et al., Preparation and Properties of Al_2O_3-PF Composite Functional Protective Coating on the Surface of Polymer Matrix Composites, *Surf. Coat. Technol.*, 2023, **456**, p 129138.

21. Q.Q. Peng, M. Liu, Y.F. Huang et al., Development Mechanism and Performance of Al_2O_3-PF Composite Coating on Epoxy Resin Matrix Composite Surface by Supersonic Plasma Spraying, *Surf. Coat. Technol.*, 2022, **446**, p 128762.

22. D.L. Sun, X.C. Yu, Fundamentals of Adhesives and Bonding Technology. Chemical Industry Press, 2014

23. T.B. Qiu, Experiment Design and Data Processing. Hefei: University of Science and Technology of China Press, 2008